

Dalton Transactions

Accepted Manuscript



This is an *Accepted Manuscript*, which has been through the Royal Society of Chemistry peer review process and has been accepted for publication.

Accepted Manuscripts are published online shortly after acceptance, before technical editing, formatting and proof reading. Using this free service, authors can make their results available to the community, in citable form, before we publish the edited article. We will replace this *Accepted Manuscript* with the edited and formatted *Advance Article* as soon as it is available.

You can find more information about *Accepted Manuscripts* in the [Information for Authors](#).

Please note that technical editing may introduce minor changes to the text and/or graphics, which may alter content. The journal's standard [Terms & Conditions](#) and the [Ethical guidelines](#) still apply. In no event shall the Royal Society of Chemistry be held responsible for any errors or omissions in this *Accepted Manuscript* or any consequences arising from the use of any information it contains.

Cite this: DOI: 10.1039/c0xx00000x

www.rsc.org/xxxxxx

ARTICLE TYPE

Thin-coated water soluble CdTeS alloyed quantum dots as energy donors for highly efficient FRET

Akram Yahia-Ammar,^a Aline M. Nonat,^{*a} Anne Boos,^b Jean-Luc Rehspringer,^c Zouhair Asfari^a and Loïc J. Charbonnière^{*a}⁵ Received (in XXX, XXX) Xth XXXXXXXXX 20XX, Accepted Xth XXXXXXXXX 20XX

DOI: 10.1039/b000000x

The synthesis of highly luminescent water soluble CdTe_xS_y quantum dots (QDs) is described and their elemental composition and optical properties are fully characterized. Glutathione (GSH)-capped nanocrystals were obtained from an aqueous solution of CdCl₂, Na₂TeO₃ and GSH in the presence of NaBH₄ upon heating at 100°C. Spherical CdTe_xS_y alloyed nanoparticles with diameters ranging from 2 to 4 nm were formed, and characterized by X-ray powder diffraction and Transmission Electron Microscopy. Their elemental composition was determined from Inductively Coupled Plasma Atomic Emission Spectroscopy and CHN elemental analysis experiments. A model for the determination of their molecular formulas, molecular weights and extinction coefficients is proposed. Surface GSH molecules were involved in amide bond formation with fluorescent Nile-Red molecules, to be used as energy acceptor in Förster resonance energy transfer (FRET) experiments. FRET was observed from the CdTe_xS_y core ($\lambda_{\text{ex}} = 430$ nm) to the Nile-Red dye ($\lambda_{\text{em}} = 648$ nm) with an almost quantitative FRET efficiency ($\eta_{\text{FRET}} = 98\%$). A detailed analysis of the FRET is presented, revealing a core-dye distance of 24 Å, in very good agreement with the estimated radius of the core (13 Å) as measured by TEM. The QDs present excellent photophysical properties (QY up to 29%), easy synthesis and can be isolated as solids and redispersed in water without loss of their photoluminescence efficiency.

1. Introduction

Fluorescent nanocrystals with semiconductor material, also called Quantum Dots (QDs),¹ have been found to outperform traditional organic fluorescent dyes in many ways (e.g. size-tunable optical properties, high quantum yields and high extinction coefficients). Moreover, they are strongly resistant to photo-bleaching, which make them ideal agents for many applications in various fields including electronic and optoelectronic devices² such as solar cells,³ photo detectors, transistors, or as bio-imaging probes or sensors for optical imaging and diagnostics.^{4,5,6} Indeed, the size of the QDs (from few nm to 30 nm) is compatible with the labeling of biomolecules for targeted fluorescence imaging^{7,8} and, more particularly, for the detection and quantification of a large variety of analytes by Time-Resolved Förster resonance energy transfer (FRET) bioassays.^{9,10,11,12,13}

QDs have emerged as excellent tools for FRET experiments, either as energy acceptor^{14,15} because of their broad absorption spectrum, or as energy donors^{16,17} because they possess size-tunable narrow emission with high quantum yields. The sensitivity of such FRET experiments can be greatly improved by optimizing several parameters among which the FRET efficiency, which can be achieved by minimizing the distance between the donor and the acceptor.¹⁸ Therefore the properties of bioconjugated QDs in FRET experiment are strongly influenced by their surface chemistry. Water soluble and biofunctionalized QDs, as well as commercially available QDs, are very often obtained from organic media and are coated with a polymer, which is meant to improve the solubility and stability of the QDs in biological media. The coating significantly increases the size

of the nanoparticles in comparison to the semiconducting core and as a consequence, the QDs/analyte distance. Replacing the thick polymer coating by a shell of small hydrophilic ligands should significantly improve the FRET efficiency. Glutathione (GSH) is a thiol-containing tripeptide found in most organisms, which possesses important anti-oxidizing properties and is implied in cellular and metabolic functions including amino acid transport, neuromodulation and neurotransmission.¹⁹ GSH has therefore been covalently coupled to polymer-coated quantum dots²⁰ or directly used as capping ligand for the synthesis of water soluble QDs for biological applications.^{21,22,23}

In this study, a simple aqueous synthesis of water soluble glutathione-capped CdTe_xS_y QDs is described as well as the characterization of the QDs by X-ray powder diffraction and Transmission Electron Microscopy. The elemental composition of the QDs, determined from Inductively Coupled Plasma Atomic Emission Spectroscopy and CHN elemental analysis experiments, was monitored as a function of time, together with their optical properties, in order to get a full insight into the composition and the growth mechanism of the as-obtained QDs. From these analyses, their molecular formula could be determined, giving access to their molecular weights and extinction coefficients, which are two essential parameters to determine the coupling rate in a conjugation experiment. Finally, Nile-Red dyes were covalently coupled to the GSH molecules at the surface via simple carbodiimide coupling chemistry and used as FRET acceptors. The FRET process was studied by steady-state and time-resolved spectroscopy. The challenging question of the quantification of bond-surface molecules was finally addressed since it is essential for applications in quantitative biological studies such as fluoroimmunoassays.

Experimental section

Materials and general methods

Solvents and starting materials were purchased from Aldrich, Acros and Alfa Aesar and used without further purification. ¹H and ¹³C NMR spectra were recorded on Bruker AC 200, Avance 300 and Avance 400 spectrometers operating at 200, 300 and 400 MHz, respectively. Chemical shifts are reported in ppm, with residual protonated solvent as internal reference.²⁴ IR spectra were recorded on a Perkin Elmer Spectrum One Spectrophotometer as solid samples and only the most significant absorption bands are given in cm⁻¹. High Resolution Mass spectra were recorded by electrospray ionisation method on a microTOF LC Bruker Daltonics. CHN elemental analyses were recorded on a Vario EL III from Elementar at the Service Commun

d'Analyses of the University of Strasbourg. UV-visible absorption spectra were recorded on a Specord 205 (Analytik Jena) spectrometer. Steady state emission and excitation spectra were recorded on a Horiba Jobin Yvon Fluorolog 3 spectrometer working with a continuous 450W Xe lamp. Detection was performed with a Hamamatsu R928 photomultiplier. All spectra were corrected for the instrumental functions. When necessary, a 399 nm cutoff filter was used to eliminate second order artefacts. Luminescence lifetimes were measured on the same instrument working in the Time Correlated Single Photon Counting (TCSPC) mode with a NanoLED emitting at 303 nm as the excitation source. Mono-exponential and multi-exponential emission decay profiles were fitted with the Datastation software from Jobin Yvon. The luminescence quantum yields were determined using a Hamamatsu Quantaaurus-QY integrating sphere according to the procedure described in reference 25.

Synthesis of the functionalized Nile-Red dye

Compound 1⁴⁵ and tert-butyl(3-bromopropyl)carbamate^{26,27} have been synthesized according to procedures from the literature. **Compound 2:** NaH (28.0 mg, 69.60 mmol) was added to a solution of compound 1 (450.0 mg, 0.99 mmol) in 5 mL anhydrous DMF under argon and the mixture was stirred at room temperature for 20 minutes. Tert-butyl(3-bromopropyl)carbamate (280 mg, 1.17 mmol) was added and the reaction mixture was stirred for 20 h at 36°C under argon. The crude product was extracted with CH₂Cl₂ (3×80 mL) and the organic layer was collected, dried over MgSO₄ and evaporated to dryness under reduced pressure. The residual material was purified by flash column chromatography eluting with a CH₂Cl₂/MeOH gradient from 0% to 1.5% MeOH in 40 min to afford 2 as a red solid (230 mg, 40%). ¹H NMR (300 MHz, CDCl₃) δ 8.15 (d, 1H, *J* = 8.7 Hz), 7.98 (d, 1H, *J* = 2.6 Hz), 7.57 (d, 1H, *J* = 9.0 Hz), 7.13 (dd, 1H, *J*₁ = 8.7 Hz, *J*₂ = 2.6 Hz), 6.63 (dd, 1H, *J*₁ = 8.7 Hz, *J*₂ = 2.6 Hz), 6.44 (d, 1H, *J* = 2.6 Hz), 6.24 (s, 1H), 4.93 (s, 1H), 4.20 (t, 2H, *J* = 6.0 Hz), 3.77 (t, 4H, *J* = 7.1 Hz), 3.72 (s, 6H), 3.38 (m, 2H), 2.67 (t, 4H, *J* = 7.1 Hz), 2.06 (m, 2H), 1.45 (s, 9H). ¹³C NMR (75 MHz, CDCl₃) 183.3, 171.9, 161.7, 156.2, 151.8, 149.9, 146.6, 141.6, 133.9, 131.2, 127.9, 125.9, 125.3, 118.7, 109.7, 107.0, 105.9, 97.4, 79.4, 66.2, 52.1, 47.1, 38.0, 32.2, 29.7, 28.6. IR (neat) 3442, 2960, 2362, 1741 cm⁻¹. MS (ESI): 608.26 [M + H]⁺ (33%), 630.24 [M + Na]⁺ (67%). Anal. Calcd (mass %) for C₃₂H₃₇N₃O₉: C, 63.25; H, 6.14; N, 6.92 Found: C, 63.09; H, 6.31;

N, 6.80.

Compound 3: TFA (1.3 mL) was added to a solution of 2 (150 mg, 0.24 mmol) in CH₂Cl₂ (6 mL) and the mixture was stirred at room temperature for 30 min. The mixture was evaporated to dryness under reduced pressure and purified by flash column chromatography eluting with an isocratic mixture of CH₂Cl₂/MeOH 94/6 to afford 3 as a red solid (100 mg, 82%). ¹H NMR (400 MHz, MeOD) δ 8.02 (d, 1H, *J* = 8.8 Hz), 7.99 (d, 1H, *J* = 2.2 Hz), 7.54 (d, 1H, *J* = 9.1 Hz), 7.18 (dd, 1H, *J*₁ = 8.8 Hz, *J*₂ = 2.4 Hz), 6.80 (dd, 1H, *J*₁ = 9.1 Hz, *J*₂ = 2.4 Hz), 6.61 (d, 1H, *J* = 2.4 Hz), 6.20 (s, 1H), 4.30 (d, 2H, *J* = 5.7 Hz), 3.81 (t, 4H, *J* = 7.0 Hz), 3.72 (s, 6H), 3.25 (t, 2H, *J* = 7.2 Hz), 2.71 (t, 4H, *J* = 7.0 Hz), 2.26 (m, 2H). ¹³C NMR (100 MHz, MeOD) δ 185.0, 173.7, 162.8, 153.9, 152.3, 147.9, 140.9, 135.3, 132.3, 128.6, 126.6, 126.2, 119.3, 111.9, 107.9, 105.4, 98.3, 66.6, 52.4, 48.0, 38.5, 32.9, 28.3. MS (ESI): 508.21 [M + H]⁺. IR (neat) 3383, 2967, 2362, 1729 cm⁻¹. Anal. Calcd (mass %) for C₂₇H₂₉N₃O₇·0.6TFA: C, 57.86; H, 5.10; N, 7.18 Found: C, 57.84; H, 5.67; N, 7.26.

Preparation of CdTe_xS_y QDs

In a two-neck flask were added 80 mL of a CdCl₂ solution in ultrapure water (0.04 M, 3.2 mmol), trisodium citrate dihydrate (2.0 g, 6.8 mmol) and 1 L of ultrapure water. L-glutathione (1.0 g, 3.3 mmol), 40 mL of a Na₂TeO₃ solution in water (0.01 M, 0.4 mmol) and NaBH₄ (1.0 g, 26.4 mmol) were added under vigorous stirring. The pH of the solution was 9.4. After stirring at room temperature for 1h30, the mixture was heated at 100°C. Upon heating, three aliquots were taken after 2h (350 mL, **QD540**), 4h (350 mL, **QD600**) and 10h (420 mL, **QD650**). The nanocrystals were precipitated by addition of EtOH (1L) and the precipitates were separated by centrifugation, washed with EtOH and dried under vacuum to obtain **QD540** (395 mg), **QD600** (230 mg) and **QD650** (240 mg) as powders, with maximum emission wavelengths at 540 nm, 600 nm and 650 nm, respectively. The procedure was repeated, taking seven samples of 100 mL after 1h heating, 2h, 3h, 3h30, 4h30, 6h20 and 7h20, respectively. Powders were obtained by precipitation with EtOH. The extinction coefficients have been measured from two independent measurements of solutions of quantum dots with known concentrations. The corresponding concentrations have been calculated from precise weighing of the compounds by using the chemical formula given in Table 3.

Solid-state characterization of the QDots

Inductively Coupled Plasma Atomic Emission Spectroscopy (ICP-AES) analysis of samples in water were performed with a Varian 720 spectrometer equipped with a quartz Meinhard nebulizer and a cyclone spray chamber. Samples were mineralized with nitric acid on a sand bath for approximately 1 h prior to analysis. Cd, Te and S emission were measured at two to three wavelengths: 214.439 nm and 226.502 nm for Cd, 180.669 nm, 181.972 nm and 182.562 nm for S and 182.153 nm, 214.282 nm and 238.579 nm for Te. Calibration of the instrument was performed with standards prepared from 1000 mg·L⁻¹ certified standards (CPI international) or from dilution of a stock solution of Na₂TeO₃ in water.

X-ray diffraction (XRD) measurements were carried out on a D8 Advance Bruker diffractometer in a θ/2θ mode and using the

Cu-K α 1 radiation at 1.5406 Å.

Transmission electron microscopy (TEM) images were recorded with a TOPCON model 002B transmission electron microscope coupled with energy dispersive X-ray (EDX) spectroscopy, operating at 200 kV, with a point-to-point resolution of 0.18 nm. Powder samples were dispersed in ethanol and a drop of this suspension deposited on TEM grids. The grid was prepared with a porous membrane covered by an amorphous carbon layer. In order to avoid disturbing random signal coming from amorphous carbon, detected CdTe $_x$ S $_y$ particles were those which lies on strand of these holes.

Coupling of the Nile-Red dye on QDs

A solution of CdTe $_x$ S $_y$ QDs emitting at 540 nm (1.6×10^{-5} M) was prepared by dissolving 12.6 mg of **QD540** in 10 mL TRIS-HCl buffer 0.01M at pH 7.4. To this solution were added EDC (58 mg, 0.37 mmol) and NHS (18 mg, 0.18 mmol) and the mixture was stirred at room temperature for 20 min. From this stock solution, six batches of 1 mL were prepared. A stock solution of Nile-Red in methanol (2.5×10^{-2} M) was prepared by dissolving 12.8 mg in 1 mL. Aliquots of 3 μ L (5 eq.), 6 μ L (9 eq.), 9 μ L (13 eq.), 12 μ L (18 eq.), 15 μ L (23 eq.) and 24 μ L (37 eq.) were respectively added to the batches of activated **QD540**. The solutions were stirred at 30°C for 45 minutes and the functionalized QDs were precipitated by addition of methanol, separated by centrifugation, washed with methanol (20 cycles) and dried under vacuum.

In order to determine the influence of Nile-Red dye in non-specific interaction with the surface of the CdTe $_x$ S $_y$ QDs, a control experiment was performed by mixing a solution of CdTe $_x$ S $_y$ QDs emitting at 540 nm (1.6×10^{-5} M) and 15 μ L (23 eq.) of Nile-Red stock solution in methanol. The solutions were stirred at 30°C for 45 minutes and the functionalized QDs were precipitated by addition of methanol, separated by centrifugation, washed with methanol (20 cycles) and dried under vacuum.

Results and Discussion

Aqueous synthesis of the CdTe $_x$ S $_y$ QDs

Glutathione-capped water-soluble CdTe $_x$ S $_y$ were easily obtained by a one-step synthetic route from cadmium chloride (4 eq.), glutathione (GSH, 4 eq.) and a telluride precursor, which was obtained from the reduction of Na $_2$ TeO $_3$ (0.5 eq.) by NaBH $_4$ (32 eq.) at room temperature, by optimization of a procedure similar to the one reported by Chi and co-workers.²⁸ It is to be noticed that, despite numerous efforts, we have not been able to reproduce the very high 86% quantum yield reported in this work. In a first step, the synthesis was performed with various Cd:Te:GSH stoichiometric ratios ($x : y : z$ with $x = 4$; $0.2 \leq y \leq 3$ and $z = 4$ or 8). For the highest telluride contents ($y \geq 1.5$), the formation of aggregates was observed, resulting in the measurements of low quantum yields. However, when the ratio of Te $^{2-}$ is too low ($y = 0.2$), or in the presence of an excess of GSH ($z = 8$), the obtained QDs are characterised by a large proportion of CdS. This is emphasized by the presence of a typical absorption band at 380 nm in the UV absorption spectra and with lower photoluminescence quantum yields (PLQY <20% at 600 nm). Optimal conditions in terms of reproducibility of the

experiment and quantum yields were obtained for a 4:0.5:4 stoichiometry. A sodium citrate buffer (at pH 9.4) was used in order to stabilize the obtained nanocrystals by electrostatic repulsion of the negatively charged carboxylate side-chains of the GSH ($pK_{a1} = 3.59$, $pK_{a2} = 8.75$, $pK_{a3} = 9.65$).²⁹ At room temperature, the Te precursor reacts with the Cd-GSH complex to form a green solution of GSH-capped CdTe QDs, which start to grow when refluxing at 100°C, as observed from the colour change of the solution from green to orange and finally red. The reaction was stopped, when the size corresponding to the desired emission wavelength was achieved and the QDs were isolated as luminescent powders by precipitation with EtOH. The temporal evolution of the reaction can easily be monitored by UV-Vis absorption spectrometry and photoluminescence. The evolution of the UV-Vis spectra as well as the corresponding emission spectra for a 4:0.5:4 Cd:Te:GSH stoichiometry is displayed in Figure S1. In a large scale synthesis, three batches of nanoparticles were isolated at different reaction times: 2h, 4h and 10h for **QD540**, **QD600** and **QD650** (where the numbers refer to the emission wavelengths of the quantum dots), respectively. The corresponding absorption and emission spectra are displayed in Figure 1. Noteworthy, the isolated solid samples were stable for months at ambient temperature. Only the larger **QD650** sample showed traces of degradation after 5 months.

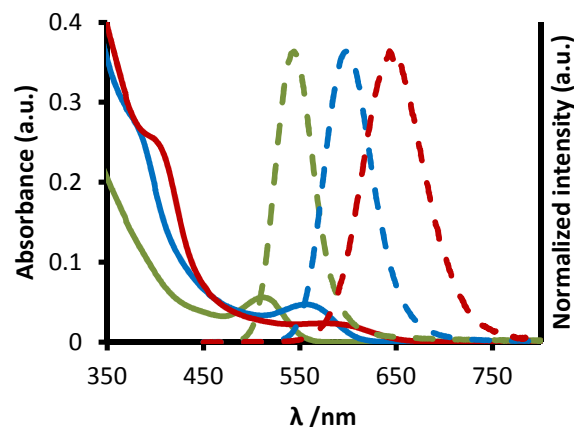


Figure 1 Evolution of the absorption (full lines) and intensity-normalized emission spectra (dashed lines, $\lambda_{ex} = 430$ nm) of the CdTe $_x$ S $_y$ -GSH QDs in 0.01 M TRIS-HCl (pH 7.4) at three different reaction times (2h, **QD540**, in green, 4h, **QD600**, in blue, 10h, **QD650**, in red).

Optical properties of the CdTe $_x$ S $_y$ QDs

Emission patterns have been measured with full width at half-maximum (FWHM) of 46 nm, 59 nm and 70 nm, for **QD540**, **QD600** and **QD650**, respectively, which are typical of QDs with narrow-size distribution (Figure 1). Upon heating, absorption and emission maxima are shifted towards the red region, in agreement with the increase of the particle size and the decrease of quantum confinement. Moreover for the longer reaction times, new absorption bands are observed at 375 nm for **QD600** and 400 nm for **QD650**, which correspond to absorption of CdS.²⁰ Indeed,

whereas CdTe cores can already be formed at room temperature, this is not the case of CdS, which displays a slower kinetic of formation, in line with the big differences of bond energies (as a comparison, bond-dissociation energies of $D^{\circ}(\text{Cd-Te})=100.1$ kJ/mol and $D^{\circ}(\text{Cd-S})=208.5$ kJ/mol have been reported).³⁰ Upon heating, S^{2-} obtained by the reduction of glutathione in the presence of sodium borohydride,^{22,31} is progressively incorporated at the surface of the CdTe core to form gradient alloyed CdTe_xS_y nanoparticles with a Te-rich core and a CdS-rich surface.

The luminescence quantum yields were measured by an absolute method using an integrating sphere and amount to 24%, 29% and 10%, for **QD540**, **QD600** and **QD650**, respectively (Table 1). These photoluminescence quantum yields (PLQY) are in good agreement with previously reported PLQY for GSH-CdTe QDs.²² The increase in quantum yield between **QD540** and **QD600** can be related to the growth of the protective CdS shell at the surface of the CdTe core, which reduces the non-radiative trapping by dangling bonds and defects. However, for bigger nanoparticles, the photoluminescence quantum yield starts to decrease probably due to changes in the surface states, as seen from the structural characterization (see below). Time-correlated single-photon counting decay (TCSPC) profiles (Figure S2) were recorded, upon excitation at 303 nm and fitted to tri-exponential decays, using Equation (1):

$$I(t) = \sum_{i=1}^3 A_i \exp(-t/\tau_i) \quad (1)$$

where τ_i represents the decay time and A_i represents the amplitudes of the component at $t=0$.

Intensity average decay times were calculated using Equation (2):³²

$$\langle \tau \rangle = \frac{\sum_{i=1}^3 A_i \tau_i^2}{\sum_{i=1}^3 A_i \tau_i} \quad (2)$$

Table 1 Lifetimes τ_i ($i=1-3$), corresponding populations B_i ($i=1-3$), average lifetimes $\langle \tau \rangle$ and luminescent quantum yields of the as-prepared **QD540**, **QD600** and **QD650**.

	$\tau_1(\text{ns})/B_1(\%)$	$\tau_2(\text{ns})/B_2(\%)$	$\tau_3(\text{ns})/B_3(\%)$	$\langle \tau \rangle$ (ns)	Φ (%)
QD540	12 (4.4)	38 (71.5)	93 (24.1)	50	24
QD600	8 (3.8)	42 (71.1)	95 (25.1)	54	29
QD650	6 (2.9)	44 (36.6)	122 (60.5)	90	10

All results are summarized in Table 1. The fast component (6-12 ns) is associated with exciton recombination in the core of the nanoparticles and the longer components (37 -122 ns) are considered to originate from thermal deactivation of the surface states.³³ The slow component increases with the emission wavelength, due to a decrease of the surface/volume ratio and also to the formation of a CdS rich layer. Such influence has already been reported for CdTe/CdS³⁴ and CdTe/CdSe³⁵ core-shell nanoparticles. The lifetime lengthening in such type II structures is well explained by the reduction in the non-radiative decay channel due to the separation of the charge carriers. We can postulate that a similar phenomenon is observed to a lesser

extent in gradient-alloyed structures. As a comparison, average lifetimes of 21 ns and 24 ns have been reported for green and red emitting TGA-capped CdTe NPs, with maximum emission at 553 nm ($\tau_1 = 11$ ns (41%), $\tau_2 = 28$ ns (59%)) and 650 nm ($\tau_1 = 11$ ns (32.1%), $\tau_2 = 31$ ns (67.9%)), respectively.³⁶ A significant increase is observed for our NPs, which might be related to the presence of the CdS protecting shell.

5.5 Structural characterization of the CdTe_xS_y QDs

Crystalline spherical nanoparticles were observed by TEM and HR-TEM (Figure S3). The average diameter was estimated to 3.1 ± 0.8 nm, for the QDs emitting at 540 nm. According to previous report,³⁷ the average size of the CdTe_xS_y core can be estimated from the first excitonic absorption band (λ) by using Equation (3), as described by X. Peng *et coll.*, within the approximation of pure CdTe cores.³⁸ A good correlation was observed between the experimental diameter measured by HR-TEM ($D_{Exp} = 3.1$ nm) and the theoretical diameter obtained by empirical fitting ($D_{Th} = 3.3$ nm).

$$D_{Th} = (9.8127 \times 10^{-7} \times \lambda^3) - (1.7147 \times 10^{-3} \times \lambda^2) + (1.0064 \times \lambda) - 194.84 \quad (3)$$

The XRD diffraction patterns of the as-prepared CdTe_xS_y QDs were also recorded and are in good agreement with literature data (Figure 2).³⁹ The sample emitting at 540 nm displays a peak at 25° (111) and a broad band at *ca.* 45° due to overlap of the (220) and (311) diffraction bands, confirming that the QDs have a zinc blend structure. It has to be noticed that the positions of the peak maxima are progressively shifted towards the bigger angles with the size of the dots due to the presence of a significant amount of CdS.⁴⁰ As expected, the diffraction peaks are sharpening with the size of the nanocrystals and with the proportion of CdS, leading to peaks close to pure CdS for sample **QD650**.

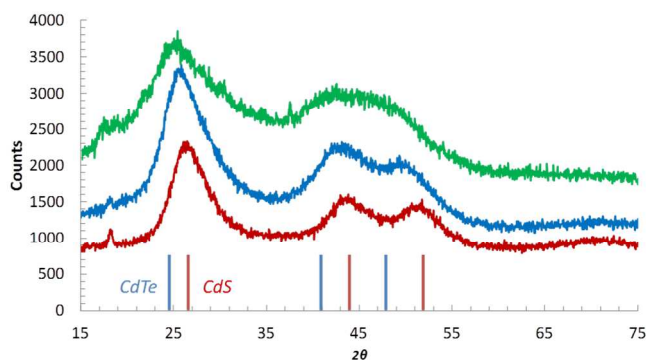


Figure 2 XRD patterns of the alloyed CdTe_xS_y -GSH QDs: **QD540** (green), **QD600** (blue) and **QD650** (red) with the peak positions of zinc blende CdTe (blue, international table 03-065-1046) and CdS (red, 03-065-2887).

The elemental composition of the QDs was determined from Inductively Coupled Plasma Atomic Emission Spectroscopy combined with CHN elemental analysis experiments (Table 2). The molar ratio of Cd, Te and S (S_{tot}) were determined by ICP-AES, the molar ratio of GSH at the surface (S_{GSH}) was determined from CHN analysis and the molar ratio of S in the core, S_{Core} , was calculated as $S_{Core} = S_{tot} - S_{GSH}$. Knowing the

proportion of CdTe and CdS in the core, it was assumed that the density of the core of these spherical nanocrystals is equal to the weighted average density of CdTe and CdS. The molecular weight of the core could thus be determined from the core diameters previously determined (Scheme 1). Taking into account the molar ratios determined by elemental analysis, this enabled the determination of the molecular composition per QD core as well as the calculation of the number of capping GSH molecules. From these results, the total molecular weights, *i.e.* the weight of one mole of QD could be determined as well as the chemical formulas. Values are summarized in Table 3.

Table 2 Elemental composition and molar ratios of the GSH-CdTe_xS_y QDs at three different reaction times (QD540, QD600, QD650).

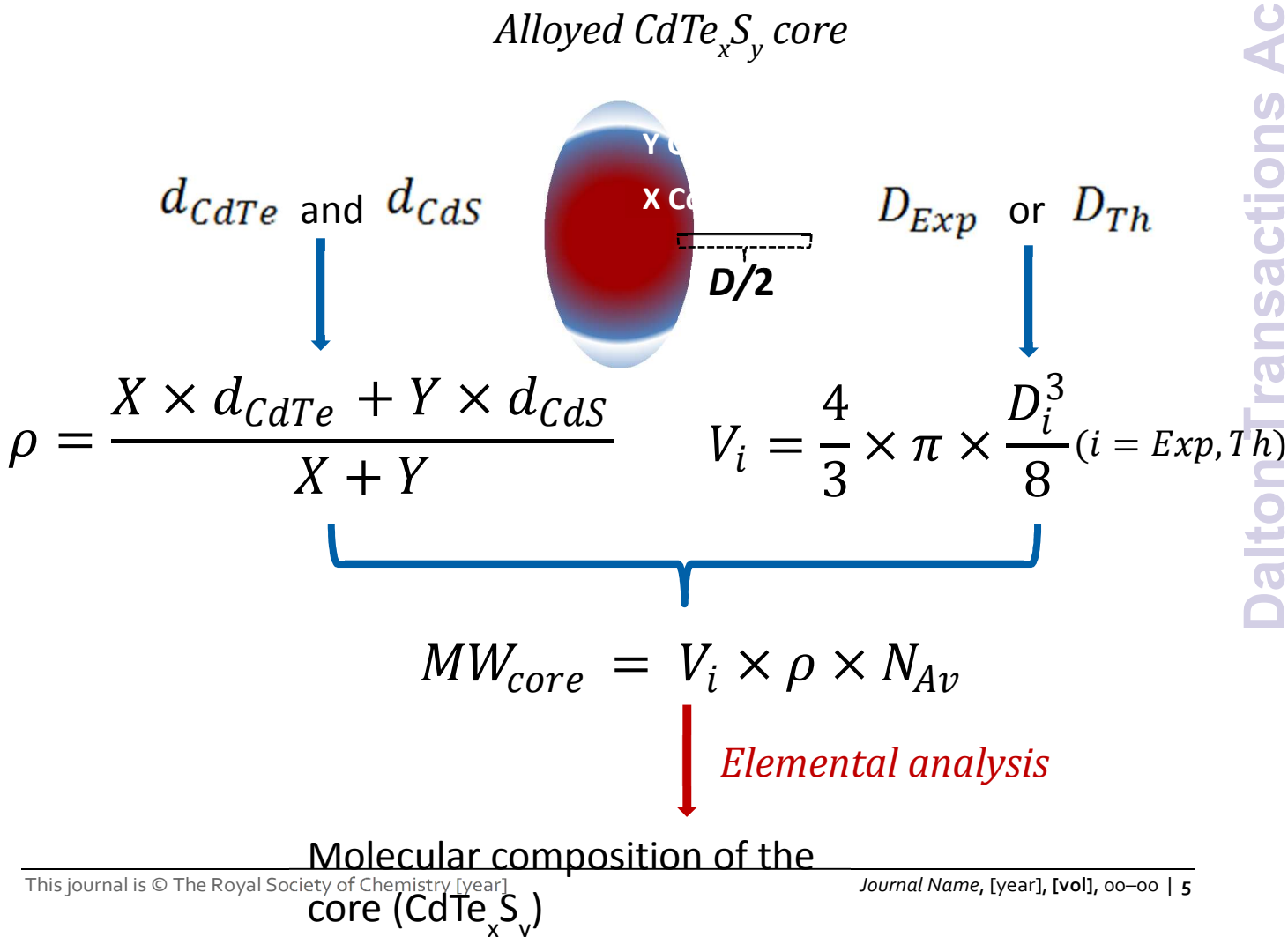
Sample	QD540	QD600	QD650
Cd (mmol/g)	2.22(5)	3.8(1)	4.81(1)
Te (mmol/g)	0.31(1)	0.58(1)	0.50(1)
S _{tot} (mmol/g)	2.11(3)	3.32(6)	4.3(1)
S _{GSH} (mmol/g)	1.56	1.07	0.55
S _{core} (mmol/g)	0.55	2.25	3.75
Cd/ (Te+S _{tot})	0.91	0.97	1
GSH/Cd	0.7	0.3	0.1

Scheme 1 Model for the determination of the molecular weights and chemical formulas of the CdTe_xS_y QDs.

Table 3 Chemical formulas of the CdTe_xS_y-GSH QDs at three different reaction times, the corresponding density (ρ), diameters (D , T_h = obtained from Equation 3 and Exp = measured by TEM), volumes (V), and their molecular weights: MW (total molecular weight), MW_{core} (of the CdTe_xS_y core only) and total number of GSH per QD.

Sample	QD540	QD600	QD650
ρ (kg/dm ³)	5.2	5.0	4.9
D_{Th} (nm)	2.6	3.3	3.3
D_{Exp} (nm)		3.1	
V_{Th} (nm ³)	9.16	18.69	19.51
V_{Exp} (nm ³)		15.89	
MW _{core} (g/mol)	28680	56640	58070
$N_{GSH/QD}$	142	106	44
MW (g/mol)	77530	93100	73200
Chemical Formula	CdTe _{0.14} S _{0.24} (GSH) _{0.69}	CdTe _{0.16} S _{0.6} (GSH) _{0.28}	CdTe _{0.15} S _{0.78} (GSH) _{0.11}

The molar ratio of Cd to total counter ions (Te + S_{tot}) was found to be close to 1. Moreover, results show that an increasing



amount of S^{2-} is incorporated upon heating, which further confirms the UV-absorption data and suggests that CdS is formed at the periphery of the nanoparticles. The total number of GSH molecules as a function of the nanoparticle size is depicted as red crosses in Figure 3, together with the results of a second synthesis (blue crosses in Figure 3), in which more aliquots were taken and their composition was similarly determined from CHN and ICP-AES analysis, as described previously. Structural and optical parameters are shown in Table S1 and Figure 3. For both syntheses, the smallest QDs ($D \leq 3.2$ nm) are characterized by the presence of a large number of GSH molecules at the surface. However, for QDs with theoretical diameters ranging from 3.2 nm to 3.3 nm, the number of GSH molecules starts to drop dramatically, which is explained by the decomposition of the GSH and its progressive incorporation in the QD to form a CdS surface-rich alloy. In order to study the influence of the ligand coating on the optical properties, the quantum yields of all the isolated quantum dots in water have been measured and reported in Figure 3 (red and blue triangles), as a function of the diameter of the core and the number of surface GSH ligands. Here again, it appears that both syntheses indicate a similar trend: for nanoparticles with diameters of *ca.* 3.3 nm and below (which are obtained during the first 4 h of reaction), the quantum yields increase with the diameter of the nanoparticles, which, as mentioned before, is probably due to the formation of a CdS surface. In both cases, maximum quantum yields were obtained after 4h of reaction, with nanoparticles of 3.3 nm diameter (29% for 4h for **QD600** and 28% at 612 nm for the second synthesis). Beyond 4 h of reaction, the nanoparticles stop to grow and their diameters remain constant (*ca.* 3.3 nm) until aggregation and precipitation is observed. Reproducible data have been obtained, which are characterised by a significant decrease of the number of GSH. For both syntheses, QDs emitting at 650 nm with luminescence quantum yield of *ca.* 10% were isolated. This sudden decrease of quantum yield followed by aggregation might also be correlated to the consumption of all the GSH introduced in the synthesis and to the apparition of surface traps due to a poor passivation of the surface by the ligands.

In order to confirm that hypothesis, the theoretical number of ligands needed to achieve complete mono-shell coverage of the quantum dots by the GSH as a function of the diameter of the core, has been estimated by an adaptation of the equation recently developed by Gaponik, Resch-Genger, Eychmüller *et al* (Equation 4) to describe a monolayer ligand shell on TGA-capped CdTe nanocrystals.⁴¹

$$N_{\text{Ligand}} = (4\pi(r_{\text{Particle}} + z_{\text{max}})^2)/A_{\text{Ligand}} \quad (4)$$

where r_{particle} is the measured radius of the spherical nanoparticles, z_{max} is the maximum height of the GSH which has been estimated to be 9.6 Å and A_{Ligand} is the area covered by the ligand in the approximation of a conical form from a space-filling MM2 model ($A_{\text{Ligand}} = 154 \text{ \AA}^2$, see Supporting Information). The theoretical curve is depicted as a black line in Figure 3. Interestingly, the number of glutathione molecules at the surface of the most emissive QDs (**QD600**, $D = 3.3$ nm, Table 3) was found to be 106, which is in very good agreement with the maximum number of ligands $N_{\text{Ligand}} = 111$ estimated from the equation. This result indicates that the surface of the most

emissive QDs is well passivated by a mono-shell ligand coverage. However, for the smallest QDs, a larger number of GSH is present at the surface, which remains constant after several precipitation steps and after size-exclusion column chromatography on Sephadex LH-20 resins. This is indicating that all GSH molecules are tightly bonds to the QDs surface, probably by the formation of an additional ligand shell.⁴¹ As expected, the largest quantum dots (**QD650** and others with $D > 3.3$ nm) are characterised by an insufficient ligand coverage, which is accompanied by a decrease of the photoluminescence quantum yield.

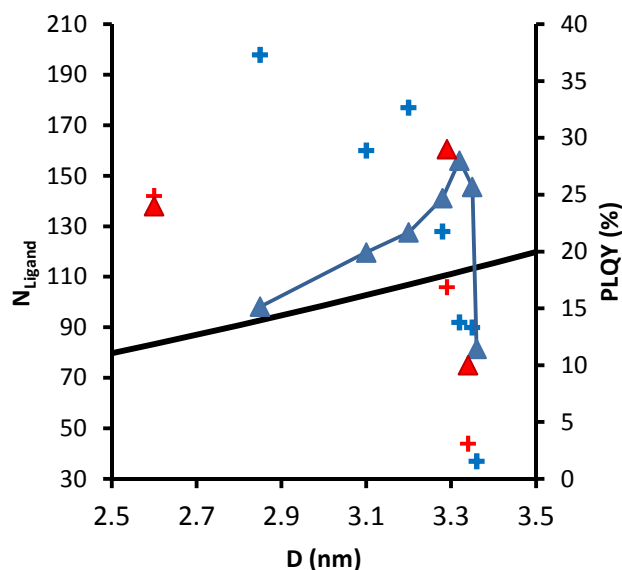


Figure 3 Estimated number of GSH per QD for a total coverage of the nanocrystals surface according to Equation 4 (black line)⁴¹ and calculated data from elemental analysis (+) for **QD540**, **QD600** and **QD650** and for similar GSH-capped CdTe_xS_y QDs of various sizes (+) obtained by the same procedure. Corresponding photoluminescence quantum yields of **QD540**, **QD600** and **QD650** (▲) and of isolated (▲) GSH-capped CdTe_xS_y QDs of various sizes obtained by the same procedure.

The QDs synthesis was also performed in the presence of larger amounts of GSH ($z = 8$), which was characterised by a stronger proportion of CdS but did not improve the luminescence properties. However, it was attempted to complete the protection of the surface by dispersing quantum dots emitting at 636 nm in the presence of an excess of GSH in water at room temperature. This led to a 11% increase of the emission quantum yield without shifting the maximum of emission (Figure S6).

On the basis of the as obtained molecular formulae, the extinction coefficients of **QD540** in water at the first excitonic absorption peak at 507 nm and at 375 nm were measured and amount to $41\,200 \text{ L}\cdot\text{mol}^{-1}\cdot\text{cm}^{-1}$ and $103\,500 \text{ L}\cdot\text{mol}^{-1}\cdot\text{cm}^{-1}$, respectively. Knowing the absorption coefficient will allow the monitoring of conjugation experiments and is also very important to get quantitative information from affinity assays in sensing applications.

The stability of the CdTe_xS_y-GSH QDs was tested in various conditions over a period of 21 days. The QDs were stable in water and at physiological pH (0.01 M TRIS-HCl, pH 7.4), which is compulsory for biological applications. Moreover the emission

properties remain constant in the concentration range 6 μM to 3 nM (Figure S4), which is of great importance as most biological applications are carried out in highly diluted conditions.⁴²

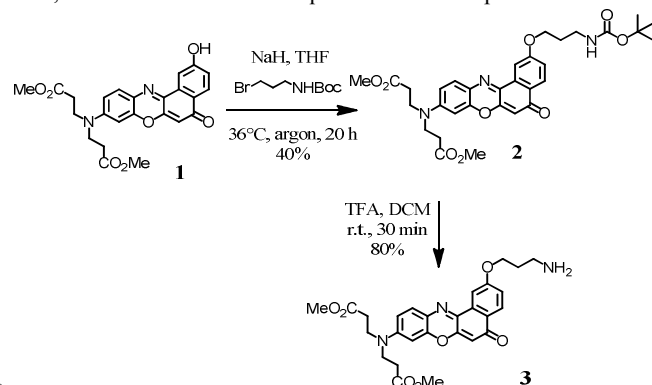
Functionalization of the QDs

5 Synthesis and optical properties of the functionalized Nile-Red dye

Recent studies have demonstrated the dynamic quenching between CdS^{43} or CdSe^{44} quantum dots as energy donors and Nile-Red dye as acceptor resulting from Coulombic interactions. Size and shape dependent energy transfer was observed with a maximum efficiency of 50% for 3.3 nm diameter CdSe QDs in chloroform. In this study, a O-functionalized Nile-Red derivative (3), has been synthesized and covalently linked to the GSH molecules on the surface of the QDs in aqueous solutions.

15 The Nile-Red derivatives 1 has been synthesized in four steps (Scheme 2) from 3-aminophenol and 1,6-dihydroxynaphthalene according to the procedure reported by Burgess *et al.*⁴⁵ The aminopropyl spacer was introduced by a nucleophilic substitution reaction of *tert*-butyl (3-bromopropyl)carbamate on the phenol group (2) followed by subsequent Boc-deprotection with trifluoroacetic acid, providing compound 3 which possesses a terminal amine that will be used for a peptidic coupling with the carboxylic acid of the GSH molecules on the QDs. The ^1H NMR spectra of 1 and 3 are displayed in Figure S7.

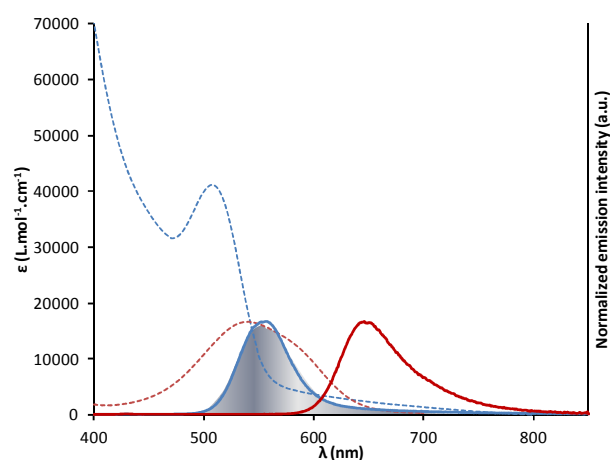
25 The absorption spectrum of the Nile-Red dye shows a peak centred at 536 nm ($\epsilon = 16\,600\ \text{M}^{-1}\text{cm}^{-1}$, Figure 4). Upon excitation at 520 nm, the Nile-Red gives rise to a red fluorescence signal centred at 648 nm (Figure 4), with a quantum yield $\phi_A = 0.09$, in 0.01M Tris-buffered aqueous solution at pH 7.4.



30 **Scheme 2** Synthesis of the functionalized Nile-Red Dye.

Covalent coupling of QD540 to the Nile-Red and characterization of the functionalized QDs

QDs emitting at 540 nm (QD540) were selected because they afford a good spectral overlap between the emission spectrum of the QDs and the absorption spectrum of the Nile-Red (Figure 4).



40 **Figure 4** Absorption (dashed lines) and emission (normalized to their maxima, full lines) spectra of the control QD540 in the presence of NHS/EDCI (blue, $\lambda_{\text{ex}} = 375\ \text{nm}$) and of the Nile-Red (red, $\lambda_{\text{ex}} = 556\ \text{nm}$). The grey area is showing the overlap between the QDs emission spectrum and the Nile-Red absorption spectrum.

The carboxylic acid functions of GSH at the surface of the QD540 were activated by NHS/EDCI⁴⁶ to lead NHS-activated QDs which were covalently coupled with the Nile-Red dye 3. After completion of the reaction, remaining dye, coupling reagents and NHS by-products were washed with methanol and removed by centrifugation. The labelling efficiency was determined by monitoring the changes in the UV-Vis absorption spectra. A series of six samples (QD-NR1 to QD-NR6) were prepared by using increasing concentration of Nile-Red together with a reference sample in which no Nile-Red was added. The absorption spectra of the labelled QDs are displayed in Figure 5. The number of dyes per QDs was calculated from the fit of the whole absorption spectra to a linear combination of the reference sample and Nile-Red contributions (Table 4). The fitting procedure as well as the corresponding spectra are detailed in the Supporting Information (Table S2 and Figure S8).

The maximum coupling was achieved upon addition of 37 eq. per QDs, with 1.86 bound Nile-Red molecules per quantum dot (Table 4). A control experiment was performed by mixing QD540 with a Nile-Red solution (23 eq.) without coupling reagents. After precipitation and washing steps, the emission spectrum was recorded (Figure S9) and displays negligible emission of Nile-Red, in comparison to the emission recorded for covalently coupled Nile-Red dyes in the same conditions (QD-NR6).

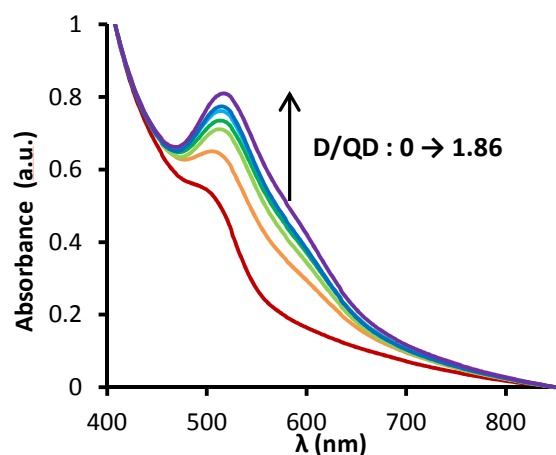


Figure 5 Absorption spectra of un conjugated (—), and of conjugated QDs with increasing NR/QD molar ratios (QD-NR1, —, QD-NR2, —, QD-NR3, —, QD-NR4, —, QD-NR5, —, QD-NR6, —) in aqueous solutions (TRIS-HCl, pH 7.4), all normalized at 408 nm.

Time-Resolved Fluorescence Study of the FRET

Exciting the QDs at 375 nm ($\epsilon = 103\,500\text{ M}^{-1}\text{cm}^{-1}$ at 375 nm) gave rise to a narrow emission of the CdTe_xS_y core centred at 540 nm. The overlap integral $J(\lambda)$ between the QDs emission spectrum and the Nile-Red absorption spectrum amounts to $9.41 \times 10^{14}\text{ M}^{-1}\text{cm}^{-1}\text{nm}^4$ (Equation S1).¹⁶ A Förster radius $R_0 = 41\text{ Å}$ (Equation S2) was found, which is very similar to the values reported for CdSe-Nile-Red pairs in chloroform ($R_0 = 51\text{ Å}$ for 2.4 nm CdSe QDs),⁴⁴ and three times bigger than the radius of the QDs core. Therefore, efficient energy transfer is expected from the CdTe_xS_y to the Nile-Red molecules at the surface.

The energy transfer from QD540 to the Nile-Red dye was studied by time-correlated single-photon counting (TCSPC) experiments. The decay profiles were recorded at the emission maxima of the QDs, at 540 nm, upon excitation at 370 nm, where the absorption of the Nile-Red dye is negligible. Upon excitation of the control NHS-activated quantum dots (QD540 in the presence of NHS/EDCI) at 370 nm, tri-exponential decay with an average lifetime of 18 ns (Table S3) was measured. The dye-conjugated QDs gave rise to multi-exponential decay profiles with shorter lifetimes (Figure S11), in agreement with the presence of an energy transfer from the CdTe_xS_y core to the Nile-Red dye. However, the tetra-exponential character of the decays renders their quantitative analysis difficult (Table S3).

Steady-State Study of the FRET

Quantitative analysis of the energy transfer was achieved by steady-state studies, upon excitation at 375 nm where the absorption of the Nile-red dye is negligible. As a control experiment, emission spectra of QD540 in 0.01 M TRIS-HCl, pH 7.4 and in presence of 0, 0.5, 1.2 and 3 equivalents of Nile-Red were recorded and typical emission of the QDs was observed (Figure S8). However, a significant contribution of the emission of Nile-red was observed at 648 nm on conjugated QDs samples (QD-NR_i, $i=1-6$). As expected, increasing the dye/QD ratio resulted in the increase of the Nile Red emission intensity relative to the QD emission intensity due to the energy transfer from the QDs to the Nile-Red dyes (Figure 6).

As a result of this energy transfer, the quenching of the control

QDs emission at 556 nm was also observed (Figure S12) and an average efficiency of the energy transfer of 98% was determined from the variations of the intensity of the QDs (Equation S3). In the case of QD-NR1, which displays a coupling ratio smaller than one, the contribution of uncoupled QDs was subtracted from the QDs emission.

The distances between the donor and the acceptor r have been calculated from Equation S4 and are summarized in Table 4. Similar nanocrystal to dye distances have been measured for all samples and they average to 24 Å, which is in very good agreement with the distance calculated as the sum of radius of the QDs core (13 Å) and the estimated distance between the sulfur atom of the glutathione and the Nile-red dye from space-filling MM2 model (14 Å, Figure S13). This distance is four times shorter than the estimated distances for non-covalent interaction between CdSe QDs and Nile Red.⁴⁴ In our case, shortening the donor-acceptor distance results in almost quantitative energy transfer efficiency, whereas a maximum of only 51% had been reached by non-covalent interaction between Nile-red derivatives and QDs in organic solvent.⁴⁴ Moreover, the donor-acceptor distance of our GSH-functionalized QDs is significantly shorter than the usual distances reported for polymer-coated quantum dots, which are in the 100 Å range.⁴⁷

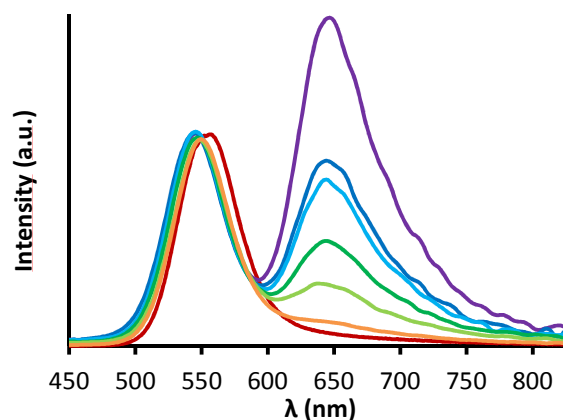


Figure 6 Emission spectra of un conjugated (—), and of conjugated QDs with increasing dye/QD molar ratios (QD-NR1, —, QD-NR2, —, QD-NR3, —, QD-NR4, —, QD-NR5, —, QD-NR6, —) normalized at the maximum emission of the QDs, 0.01 M TRIS-HCl pH 7.4, $\lambda_{\text{ex}} = 375\text{ nm}$.

Table 4 Composition of the conjugated QDs with Nile-Red and energy transfer parameters.

Sample	Dye/QD	E_{FRET} (%)	r (Å)
QD-NR1	0.80	98.4	21
QD-NR2	1.32	95.8	27
QD-NR3	1.46	97.4	25
QD-NR4	1.53	97.9	25
QD-NR5	1.59	98.1	24
QD-NR6	1.86	98.4	24

Conclusions

Highly luminescent water soluble quantum dots were synthesized by a facile and reproducible procedure in water. The tri-peptide glutathione was used as a capping ligand and the formation of gradient alloyed CdTe_xS_y QDs, which possesses a CdS rich surface, is observed. This CdS covering protects the QDs from non-radiative trapping and as a consequence, high quantum yields were observed in water (10-30%) over a broad emission spectral range (540 nm to 650 nm). The nanoparticles display narrow size distributions with diameters ranging from 2 to 4 nm and their elemental composition was determined from Inductively Coupled Plasma Atomic Emission Spectroscopy and CHN elemental analysis experiments. A model for the determination of their molecular formula, molecular weight and extinction coefficients is proposed.

Following this model and the one recently proposed by Gaponik for surface functionalization, we evidenced a strong correlation between the luminescence efficiency of the QDs and the number of GSH molecules at their surface. Whereas the optical properties are not affected by the presence of an excess of GSH (arranged as multi ligand shells), a default of GSH creates non-radiative trapping at the surface, which is associated with a decrease of the luminescence quantum yield.

Finally, the carboxylate functions of GSH have been covalently coupled to Nile-Red molecules. Förster resonance energy transfer (FRET) was observed from the CdTeS core (donor) to the Nile-Red dye (acceptor) with a quasi quantitative FRET efficiency ($\eta_{\text{FRET}} = 98\%$). A detailed analysis of the FRET allowed measuring a core-dye distance of 24 Å. This value is in very good agreement with the estimated distance from the size of the core and is significantly shorter than the usual distances reported for polymer-coated quantum dots, as for instance commercially available QDs. By combining short donor-acceptor distances and good spectral overlap, we foresee that such GSH-functionalised QDs are very good candidates for the development of FRET-based analytical tools such as fluoroimmunoassays.

Acknowledgments

This research was performed in the frame of the project “⁶⁴Cu radiolabeled nanomaterials for diagnostic and radiotherapy” (ANR) and the P2N program “NanoFRET”. This work was supported by the French Centre National de la Recherche Scientifique and the University of Strasbourg (UMR 7178). The authors thank Pascale Ronot and Salah Mebarki for performing the ICP-AES measurements, Dris Ihiwakrim for the TEM images and Mama Lafjah for her kind help with recording the DRX spectra.

Notes and references

^a Address, Laboratoire d'Ingénierie Moléculaire Appliquée à l'Analyse, IPHC, UMR 7178 CNRS/UdS, ECPM, Bât R1N0, 25 rue Becquerel, 67087 Strasbourg Cedex 02, France. Fax: +33 (0)3 68 85 27 25; Tel: +33 (0)3 68 85 26 99; E-mail: aline.nonat@unistra.fr, l.charbonn@unistra.

^b Laboratoire de Reconnaissance et Procédés de Séparation Moléculaire, IPHC, UMR 7178 CNRS/UdS, ECPM, Bât R1N0, 25 rue Becquerel, 67087 Strasbourg Cedex 02, France.

^c Département de Chimie et des Matériaux Inorganiques, IPCMS, UMR 7504, CNRS/UdS, 23 rue du Loess, BP 20, F-67037 Strasbourg, France.

† Electronic Supplementary Information (ESI) available: [Figure S1-S13, Table S1-S3, Approximation of the area covered by the GSH from a space filing MM2 model. Calculation of the Dye/QD ratios of QD-NR1, QD-NR2, QD-NR3, QD-NR4, QD-NR5 and QD-NR6 from their UV-absorption spectra, Background FRET theory and equations]. See DOI: 10.1039/b000000x/

- P. O'Brien, L. Pickett, *Chem. Mater.* 2001, **13**, 3843-3858.
- D. V. Talapin, J. S. Lee, M. V. Kovalenko, E. V. Shevchenko, *Chem. Rev.* 2010, **110**, 389-458.
- P. V. Kamat, *J. Phys. Chem. Lett.* 2013, **4**, 908-918.
- P. Wu, X.-P. Yan, *Chem. Soc. Rev.* 2013, **42**, 5489-5521.
- C. E. Bradburne, J. B. Delehanty, K. B. Gemmill, B. C. Mei, H. Mattoussi, K. Susumu, J. B. Blanco-Canosa, P. E. Dawson, I. L. Medintz, *Bioconjugate Chem.* 2013, **24**, 9, 1570-1583.
- I. Nann, W. M. Skinner, *ACS Nano* 2011, **5**, 5291-5295.
- C. Zhang, X. Ji, Y. Zhang, G. Zhou, X. Ke, H. Wang, P. Tinnefeld, Z. He, *Anal. Chem.* 2013, **85**, 5843-5849.
- I. L. Medintz, H. T. Uyeda, E. R. Goldman, H. Mattoussi, *Nature Materials* 2005, **4**, 435-446.
- L. J. Charbonnière, N. Hildebrandt, R. F. Ziesel, H.-G. Löhmansröben, *J. Am. Chem. Soc.* 2006, **128**, 12800-12809.
- K. D. Wegner, P. T. Lanh, T. Jennings, E. Oh, V. Jain, S. M. Fairclough, J. M. Smith, E. Giovannelli, N. Lequeux, T. Pons, N. Hildebrandt, *ACS Appl. Mater. Interfaces* 2013, **5**, 2881-2892.
- N. Hildebrandt, K. D. Wegner, W. R. Algar, *Coord. Chem. Rev.* 2014, **273-274**, 125-138.
- K. D. Wegner, S. Lindén, Z. Jin, T. L. Jennings, R. el Khoulati, P. M. P. van Bergen en Henegouwen, N. Hildebrandt, *Small*, 2014, **10(4)**, 734-740.
- K. D. Wegner, Z. Jin, S. Linden, T. L. Jennings, N. Hildebrandt, *ACS Nano* 2013, **7(8)**, 7411-7419.
- D. Geißler, S. Linden, K. Liermann, K.D. Wegner, L.J. Charbonnière, N. Hildebrandt, *Inorg. Chem.* 2014, **53**, 1824-1838.
- D. Geißler, L. J. Charbonnière, R. F. Ziesel, N. G. Butlin, H. G. Löhmansröben, N. Hildebrandt, *Angew. Chem. Int. Ed.* 2010, **49**, 1396-1401.
- A. R. Clapp, I. L. Medintz, H. T. Uyeda, B. R. Fisher, E. R. Goldman, M. G. Bawendi, H. Mattoussi, *J. Am. Chem. Soc.* 2005, **127**, 51, 18212-18221.
- L. Shi, V. De Paoli, N. Rosenzweig, Z. Rosenzweig, *J. Am. Chem. Soc.* 2006, **128**, 10378-10379.
- I. Medintz and N. Hildebrandt, editors: FRET – Förster Resonance Energy Transfer. From Theory to Applications”, Wiley-VCH, Germany 2014, ISBN 978-3-527-32816-1.
- C. A. Shaw, 1998, Multiple roles of glutathione in the nervous system. Glutathione in the nervous system. (Shaw C. A. Ed), pp 3-22, Chapter 1, Taylor & Francis, Washington DC.
- C. Tortiglione, A. Quarta, A. Tino, L. Manna, R. Cingolani, T. Pellegrino, *Bioconjugate Chem.* 2007, **18**, 829-835.
- H. F. Qian, C. Q. Dong, J. F. Weng, J. Ren, *Small* 2006, **2**, 747-51.
- Y. Zheng, S. Gao, J. Y. Ying, *Adv. Mater.* 2007, **19**, 376-380.
- Y.-F. Liu, J.-S. Yu, *J. Coll. Int. Sci.* 2010, **351**, 1-9.
- H. E. Gottlieb, K. Kottyar, A. Nudelman, *J. Org. Chem.* 1997, **82**, 7512-7515.
- M. Maiti, S. Thakurta, D. Sadhukan, G. Pilet, G. M. Rosair, A. Nonat, L. J. Charbonnière, S. Mitra, *Polyhedron* 2013, **65**, 6-15.
- E. J. Brnardic, M. E. Fraley, Inhibitors of checkpoint kinases. U.S. Patent Application 049506, Dec 6, 2007.
- T. Vilaivan, *Tetrahedron Lett.* 2006, **47(38)**, 6739-6742.
- Z. Sheng, H. Han, X. Hu, C. Chi, *Dalton Trans.*, 2010, **39**, 7017-7020.
- J. Bjerrum, G. Schwarzenbach, L. G. Sillen, Stability Constants, Chemical Society, London, 1958.
- M. Grade, W. Hirschwald, *Ber. Busen. Phys. Chem.* 1982, **86**, 899-907.

- 31 H.-J. Zhan, P.-J. Zhou, Z.-Y. He, Y. Tian, *Eur. J. Inorg. Chem.* 2012, **15**, 2487-2493.
- 32 M. Jones, J. Nedeljkovic, R. J. Ellingson, A. J. Nozik, G. Rumbles, *J. Phys. Chem. B* 2003, **107**, 11346-11352.
- 33 M. Jones, J. Nedeljkovic, R. J. Ellingson, A. J. Nozik, G. Rumbles, *J. Phys. Chem. B* 2003, **107**, 11346-11352.
- 34 Q. Zeng, X. Kong, Y. Sun, Y. Zhang, L. Tu, J. Zhao, H. Zhang, *J. Phys. Chem. C* 2008, **112**, 8587-8593.
- 35 J. Wang, I. Mora-Sero, Z. Pan, K. Zhao, H. Zhang, Y. Feng, G. Yang, X. Zhong, J. Bisquert, *J. Am. Chem. Soc.* 2013, **135**, 15913-15922.
- 36 P. Yang, N. Murase, *Adv. Funct. Mater.* 2010, **20**, 1258-1265.
- 37 M. Xue, X. Wang, H. Wang, B. Tang, *Talanta*, 2011, **83**, 1680-1686.
- 38 W. W. Yu, L. Qu, W. Guo, and X. Peng. *Chem. Mater.* 2003, **15**, 2854-2860.
- 39 Y. Zheng, S. Gao, J. Ying, *Adv. Mater.* 2007, **19**, 376-380.
- 40 X. Cai, H. Mirafzal, K. Nguyen, V. Leppert, D. F. Kelley, *J. Phys. Chem. C* 2012, **116**, 8118-8127.
- 41 S. Leubner, S. Hatami, N. Esendemir, T. Lorenz, J. O. Joswig, V. Lesnyak, S. Recknagel, N. Gaponik, U. Resch-Genger, A. Eychmüller, *Dalton Trans.*, 2013, **42**, 12733-12740.
- 42 J. B. Delehanty, K. Susumu, R. L. Manthe, W. R. Algar, I. L. Medintz, *Anal. Chim. Acta*, 2012, **750**, 63-81.
- 43 S. Sadhu, M. Tachya, A. Patra, *J. Phys. Chem. C* 2009, **113**, 19488-19492.
- 44 S. Sadhu, K. K. Haldar, K. A. Patra, *J. Phys. Chem. C* 2010, **114**, 3891-3897.
- 45 J. Jose, K. Burgess, *J. Org. Chem.* 2006, **71**, 7835-7839.
- 46 Y. M. Shan, L. P. Wang, Y. H. Shi, H. Zhang, H. M. Li, H. Z. Liu, B. Yang, T. Y. Li, X. X. Fang, W. Li, *Talanta* 2008, **75**, 1008-10014.
- 47 T. T. Nikiforov, J. M. Beechem, *Anal. Biochem.* 2006, **357**, 68-76.